Article

# Effect of La Doping on Kinetic and Thermodynamic Performances of Ti$_{1.2}$CrMn Alloy upon De/Hydrogenation

Hanbing Zhang, Jichao Ye, Xiaogang Wu, Xinwei Hu, Huazhou Hu, Chuanming Ma, and Qingjun Chen*

Read Online

ACCESS | Metrics & More | Article Recommendations

**ABSTRACT:** Development of efficient hydrogen storage materials is one of the great challenges in the area of hydrogen energy and fuel cells. Herein, a La-doped Ti$_{1.2}$CrMn alloy with high hydriding capacity (2.1 wt % H) and dehydriding capacity (1.8 wt % H) was successfully developed. The crystallographic characteristics, microstructural evolution, and hydrogen storage mechanisms of the alloy were investigated systematically. It was found that the introduction of La increased the cell volume of alloy and thus improved the hydrogenation kinetic, practical hydrogenation capacity, and cyclic property. The hydrogenation kinetic results of the La-doped alloy indicate that it exhibited a higher hydrogenation rate than that of the La-free alloy. It is ascribed to the formation of LaH$_3$, which provides a fast diffusion channel for hydrogen atoms to enter the alloy matrix. The dehydrogenation enthalpy ($\Delta H$) of the La-doped alloy was calculated by the van't Hoff equation and PCT curves to be ∼18.2 kJ/mol. The cycle test proves that the La-doped Ti$_{1.2}$CrMn alloy, due to La addition, reduces the lattice expansion and lattice stress and exhibits excellent durability.
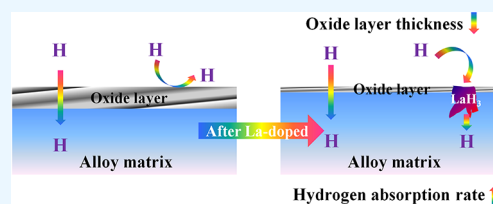
## 1. INTRODUCTION

Hydrogen is a promising energy carrier to meet the future global carbon emission reduction target.[1,2] Efficient hydrogen storage material development is a key link in hydrogen energy.[3−5] Hydrogen storage alloys have been considered as one of the most promising ways due to their high gravimetric and volumetric capacities and reasonable economics.[6−10]

Currently, the effective hydrogen storage capacity of the widely developed AB$_5$-type alloys does not exceed 1.4 wt %.[11,12] Body-centered-cubic alloys intrinsically contain higher capacities, i.e., nearly 2.4 wt %, but they have not been used for any application so far because of the high cost, difficulties in activation, and the slope in the pressure−composition−temperature (PCT) curve.[13,14] Recently, researchers found that several high-capacity materials, such as MgH$_2$, AlH$_3$, and other complex hydrides, have shown storage capacities of above 5 wt %.[15−19] However, the poor kinetics and great enthalpy change of the desorption reaction greatly hinder the practical storage application.[20,21] Numerous efforts were reported to enhance the kinetics and reduce the stability of the hydrides, such as catalysis, substitution, and nanoconfinement.[22−24]

Among various solid-state hydrogen storage materials, AB$_2$-type alloys have been extensively investigated due to their cheap cost and high volumetric content at room temperature.[25−27] Ti−Cr−Mn alloys represent one of the suitable candidates for storage hydrogen due to their high hydrogen storage capacity (2.1 wt % at −10 °C).[28] Agresti et al. and

Nong et al. also showed that TiCrMn alloy (C14 Laves phase) exhibited a more excellent hydrogen storage performance than TiCr$_2$ alloy (C15 and C14 Laves phases)[29,30] because the hydrogen storage performance of TiCr$_2$ is altered after Mn partially substituted for Cr. Hence, the single C14 Laves phase TiCrMn is regarded as a promising hydrogen storage material. However, there are still a higher plateau pressure and a lack of a systemic investigation on the microstructure evolution, kinetic, and thermodynamic mechanisms of the C14 TiCrMn intermetallic alloy upon de/hydrogenation process. Furthermore, various literature and our group research proved that rare earth doping played essential roles in shortening the activation time and ensuring a homogeneous composition.[31−33] However, the role of La doping in the high-performance Ti−Cr−Mn alloys for hydrogen storage has not been studied, especially in kinetic and thermodynamic aspects. Furthermore, La doping may increase the lattice parameters and reduce the plateau pressure as a result of the larger atomic radius of La (0.187 nm) than Ti (0.145 nm), Cr (0.125 nm), and Mn (0.137 nm) elements.
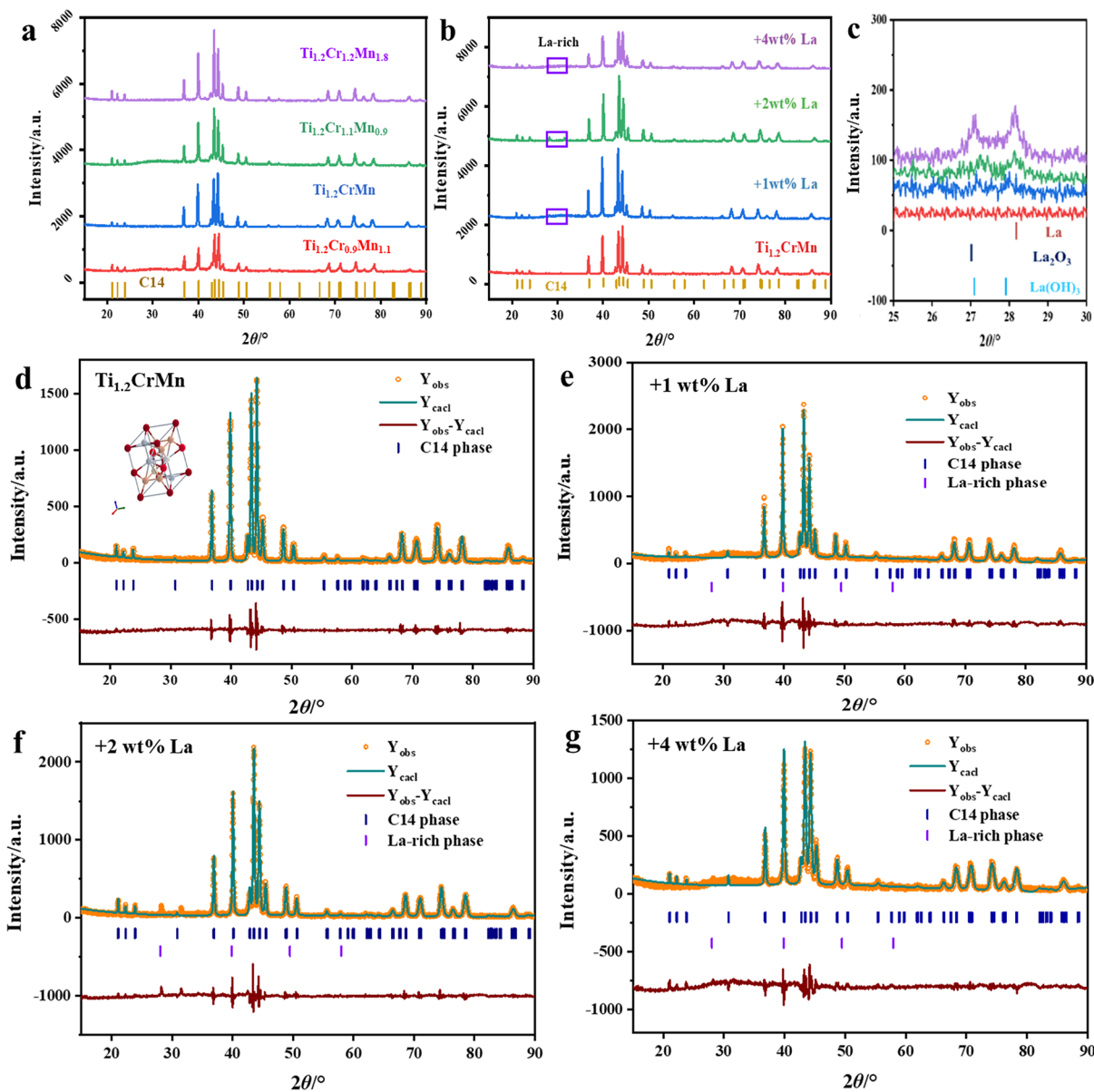
**Figure 1.** XRD patterns of the TiCrMn alloys with different (a) Cr/Mn ratios and (b, c) La doping contents and Rietveld refinement results of the (d) $Ti_{1.2}CrMn$ alloy and (e) 1 wt %, (f) 2 wt %, and (g) 4 wt % La-doped $Ti_{1.2}CrMn$ alloy.

In this study, the influence of La doping on the improvement of hydrogen storage performances of the $Ti_{1.2}CrMn$ alloy is studied in detail. The crystallographic characteristics, microstructural evolution, and hydrogen storage mechanisms of the alloys are investigated. Moreover, the doping mechanism in the kinetic and thermodynamic aspects was discussed to support further development of high-performance hydrogen storage alloys.

## 2. EXPERIMENTAL SECTION

The desired ingot alloys with a nominal composition of La-doped $Ti_{1.2}CrMn$ alloys were prepared by arc melting (WK Series Vacuum Arc Melter, Physcience, China) in an argon atmosphere (~90 A). The purity of each element exceeded 99.5 wt %. Each ingot alloy (~10 g) was smelted four times to ensure a homogeneous composition. Furthermore, an additional 3 wt % Mn was added because of the volatilization.

The phases of the La-doped $Ti_{1.2}CrMn$ alloys were identified by X-ray diffraction (XRD; Bruker D8 ADVANCE, Germany) at a scan speed of 10 °/min (15−90°) with Cu Kα radiation. The morphology and composition of the samples were characterized by a scanning electron microscope connected to an energy dispersive spectrometer (SEM-EDS; MLA650F, Bruker, Germany) and a transmission electron microscope (TEM; FEI Tecnai G2 F20, USA). After full activation at 200 °C under a rotary pump vacuum, the hydrogen storage performance of the samples was tested in a pressure−composition−temperature (PCT, Zhejiang University, China) instrument with Sievert style. Approximately 1 g of samples was kept in a vessel reactor in a glovebox. After every hydrogen absorption and desorption cycle, annealing at 200 °C under a rotary pump vacuum was performed to desorb residual hydrogen before the subsequent absorption. Furthermore, the practical hydrogen capacity was used to represent the hydrogen absorption capacity of the alloy at 300 s.

# 3. RESULTS AND DISCUSSION

## 3.1. Effect of Cr/Mn Ratios and La Doping on the Crystal Structure.
The crystal structure of alloys with

**Table 1. Effect of La Doping on the Crystal Structure of $Ti_{1.2}CrMn$ Alloys**

| samples | phase | lattice parameter $a/c$ (Å) | FWHM of (112) peak |
|---|---|---|---|
| $Ti_{1.2}CrMn$ | C14 | 4.8940/8.0359 | 0.463 |
| $Ti_{1.01}Cr_{0.84}Mn_{0.84}La_{0.01}$ | C14 + $La_2O_3$ | 4.8956/8.0390 | 0.457 |
| $Ti_{1.01}Cr_{0.84}Mn_{0.84}La_{0.02}$ | C14 + $La_2O_3$ | 4.8962/7.9772 | 0.458 |
| $Ti_{1.01}Cr_{0.84}Mn_{0.84}La_{0.04}$ | C14 + $La_2O_3$ | 4.8880/8.0200 | 0.475 |

different Cr/Mn ratios and La doping contents was characterized by XRD with monochromatic Cu K$\alpha$ radiation. It can be clearly observed that the Ti−Cr−Mn alloys with different Cr/Mn ratios are single C14 Laves (hexagonal close-packed, HCP structure), as shown in Figure 1a. Figure 1b demonstrates the effect of La doping on the crystal structure of $Ti_{1.2}CrMn$ alloy. With the increase of La content, a La-rich phase was precipitated, and the main peak of the alloy (HCP structure) in (112) was slightly shifted to the right. The La (PDF#65-1871), $La_2O_3$ (PDF#65-3185), and $La(OH)_3$ (PDF#36-1481) patterns had also been compared in Figure 1c. The correct La-rich phases in Figure 1c are the $La_2O_3$ and La phases. $La_2O_3$ is precipitated for two reasons: (1) There is often a layer of oxide skin in the raw material of electrolytic Mn and La. Due to the preferential oxygen absorption of La than other elements in the smelting process, $La_2O_3$ is formed. (2)

Since La doping significantly improves the activity of the alloy, the alloy is easily oxidized during grinding and XRD testing (exposure to the air).

As shown in Figure 1d−g and Table 1, a larger cell volume (~164 Å³) of the $Ti_{1.2}CrMn$ alloy was achieved after La doping according to the Rietveld refinement results.[34] With the increase of La doping content, the cell volume slightly increases (Table 1), which could weaken the lattice expansion of the C14 Laves phase upon de/hydrogenation. It is ascribed to the fact that the La atom has a larger atomic radius than the Ti/Cr/Mn atom. This phenomenon is consistent with the Ce-doped TiZrCrMn alloy reported in our previous work.[33] Furthermore, the effect of La doping content on the FWHM of the alloy was calculated. When the doping content of La is 1 wt %, the FWHM changes slightly. The FWHM increases with further increase in La content. It means that lattice stress and defects increase with the La content. Therefore, a suitable La doping content is important to the alloy.

A high-resolution TEM image in Figure 2a−c clearly shows a d-spacing of 0.24 nm corresponding to the (110) planes of $Ti_{1.2}CrMn$ alloy and a larger d-spacing of 0.25 nm corresponding to the (110) planes of 1 wt % La-doped $Ti_{1.2}CrMn$ alloy (Figure 2d−f), which are in good agreement with the XRD results. Furthermore, the $Ti_{1.2}CrMn$ alloy lattice shows good structure and continuity, but the lattice appears to bend after La doping, and some black regions are also observed. This is because it is difficult for La atoms to be doped into $Ti_{1.2}CrMn$ cells due to its large atomic radius. However, when lattice distortion and vacancies occur in
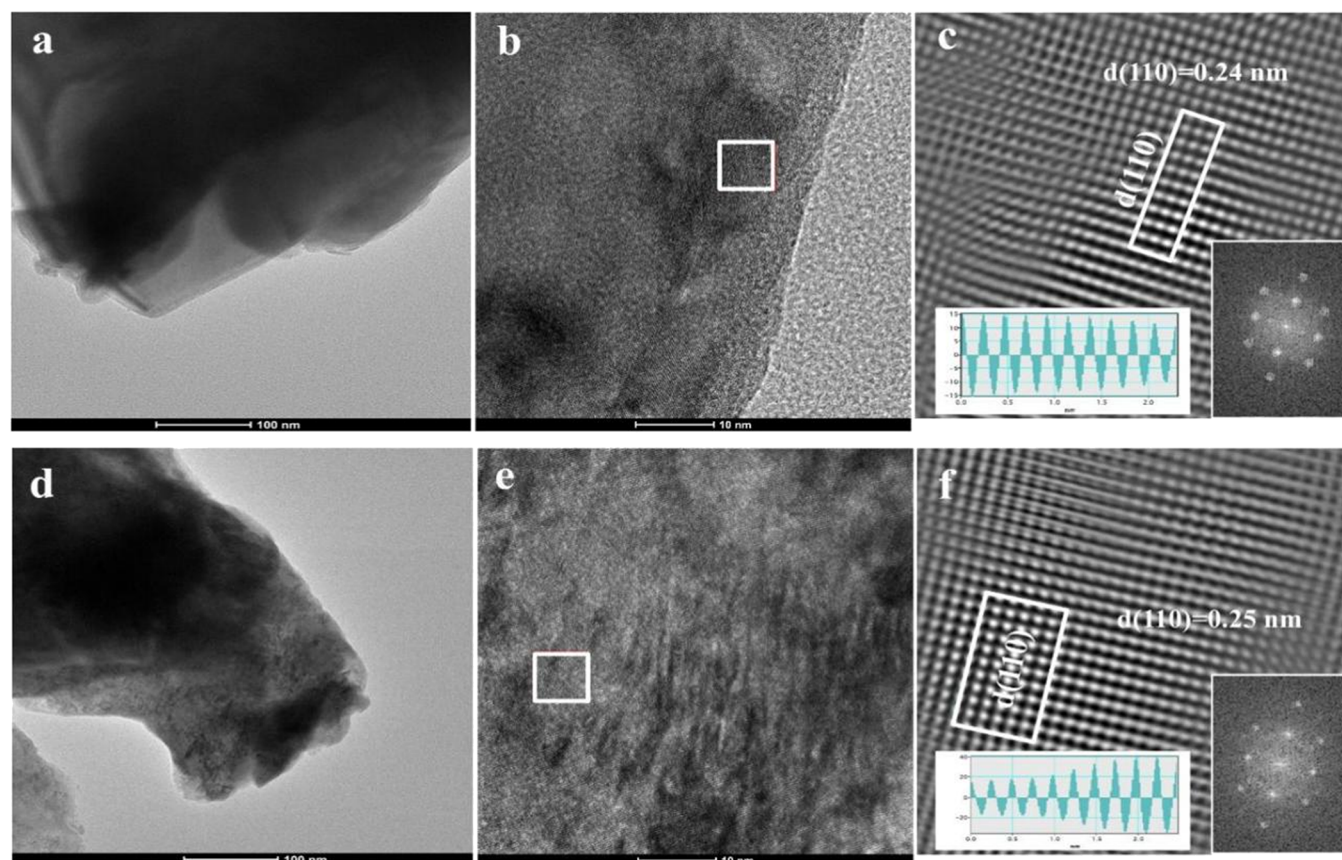


**Figure 2.** TEM images of (a, b, c) $Ti_{1.2}CrMn$ alloy and (d, e, f) 1 wt % La-doped $Ti_{1.2}CrMn$ alloy.

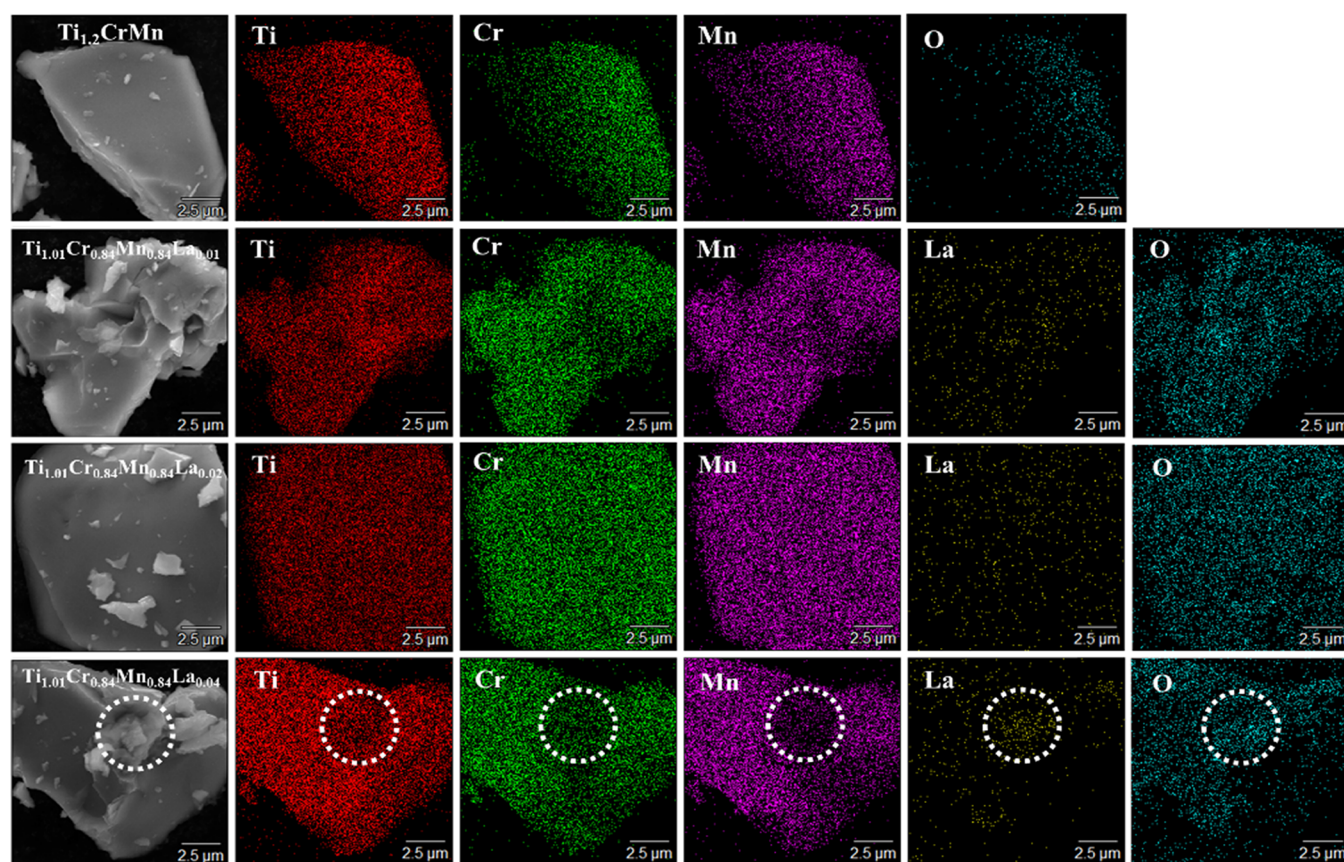**Figure 3.** SEM-EDS of $Ti_{1.2}CrMn$ alloy with different La doping contents.

$Ti_{1.2}CrMn$ alloy, part of the La could successfully dope into $Ti_{1.2}CrMn$ alloy.

**3.2. Effect of La Doping on Morphology and Composition.** SEM images and the corresponding EDS mappings of La-doped $Ti_{1.2}CrMn$ alloys with a significant difference are shown in Figure 3. With the addition of La content, the distribution of La in the alloy matrix changes from uniform to enriched. The La-doped $Ti_{1.2}CrMn$ alloy is uniformly distributed with a La content of 1 or 2 wt %. And the EDS result is also close to the designed ratio. When the content of La increases to 4 wt %, there is an obvious enrichment of $La_2O_3$ (white particles in Figure 3). The alloy composition deviates obviously from the design value, especially the La content. Because of the melting point difference between Mn (1244 °C) and $La_2O_3$ (2315 °C) in the smelting process, once the melting current increases, Mn will be volatilized seriously. The formation of $La_2O_3$ is due to the absorbed oxygen in the raw material or equipment, resulting in the poor fluidity of the alloy. When the addition amount of La is 1 wt %, there is no obvious La enrichment in the alloy. A lot of studies conclude that the improvement of the compositional homogeneity of the alloy is conducive to enhancing the hydrogen storage properties.[4,13,31] The addition of 1 wt % La does not affect the homogeneous composition (Figure 3) and phase structure (Figure 1) of the alloy, and 1 wt % La is selected as the optimum doping content.

**3.3. Hydrogenation Behaviors of Alloys with Different Cr/Mn Ratios and La Doping Contents.** The hydrogenation behaviors of Ti−Cr−Mn alloys with different Cr/Mn ratios and La doping contents were tested at 5−25 °C and an initial hydrogen pressure of 8 MPa after complete activation. As shown in Figure 4a, the practical hydrogen absorption capacities of Ti−Cr−Mn alloys were nearly 1.5 wt % in the equilibrium pressure nearly 6 MPa at 300 s. They reached practical hydrogen absorption capacities after 120 s. Figure 4b concludes that the La-doped $Ti_{1.2}CrMn$ alloy has a slight influence on the practical hydrogen absorption capacity but significantly improves the hydrogen absorption rate. To further study the influence of La doping on the hydrogen absorption rate of the alloys, the hydrogen absorption behaviors of the alloys at different temperatures were compared. Figure 4c,d depicts that the hydrogenation rates and practical hydrogenation capacities decrease with the increase of hydrogenation temperature due to the hydrogenation process being an exothermic reaction.

The specific kinetic data are further clearly summarized in Table 2. The practical hydrogen absorption time required for 1.5 wt % H of the practical hydrogen absorption of the alloys and 70% of the practical hydrogen absorption of the alloys at 300 s was decreased after slight La doping, especially in a lower reaction temperature (5 or 15 °C). It could be ascribed to the fact that La reacts preferentially with hydrogen to form hydride, which provides a fast channel for hydrogen atoms to enter the alloy matrix. The formation of $LaH_3$ was found in the XRD pattern of the hydriding $Ti_{1.01}Cr_{0.84}Mn_{0.84}La_{0.01}$ alloy, which is shown in Figure 5a. The main phase of the $Ti_{1.01}Cr_{0.84}Mn_{0.84}La_{0.01}$ alloy after hydrogenation is still the single Laves phase. The impurity peaks of the metallic La phase were transformed into $LaH_3$ ($\Delta G < 0$ at 25 °C, Figure 5b) and disappeared after hydrogenation. The impurity peaks of a small amount of $La_2O_3$ during the hydrogenation process had not changed because of $\Delta G > 0$ at 25 °C (Figure 5b).
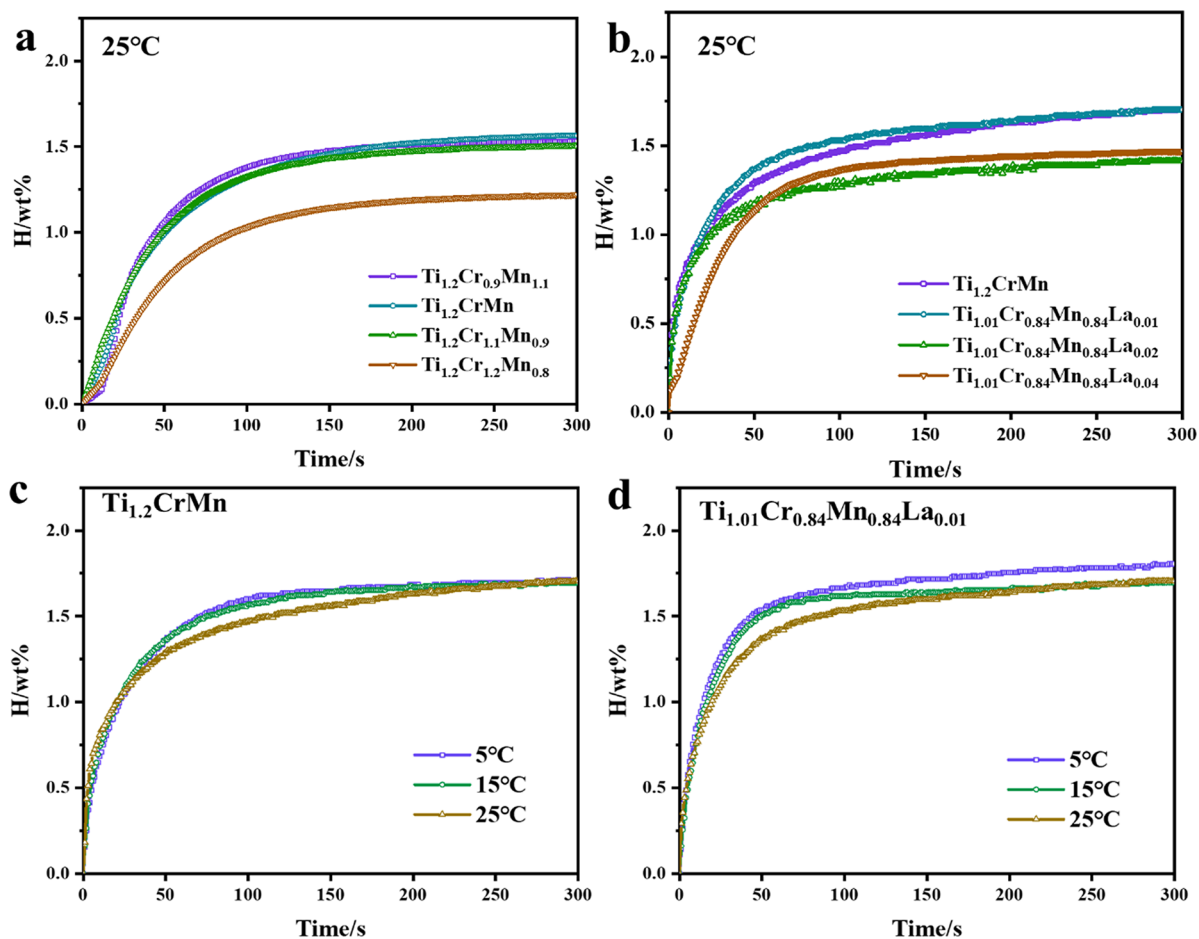
**Figure 4.** Hydrogenation kinetics of the $Ti_{1.2}CrMn$ alloy with different (a) Cr/Mn ratios and (b) La doping contents at 25 °C and the (c) $Ti_{1.2}CrMn$ alloy and (d) $Ti_{1.01}Cr_{0.84}Mn_{0.84}La_{0.01}$ alloy at different temperatures.

**Table 2. The Time Required for 1.5 wt % H of the Practical Hydrogen Absorption of the Alloys and 70% of the Practical Hydrogen Absorption of the Alloys at 300 s**

| t/s | 1.5 wt %/s | | | $T_{0.7}$/s | | |
|---|---|---|---|---|---|---|
| | 5 °C | 15 °C | 25 °C | 5 °C | 15 °C | 25 °C |
| $Ti_{1.2}CrMn$ | 72 | 75 | 116 | 35 | 32 | 40 |
| $Ti_{1.01}Cr_{0.84}Mn_{0.84}La_{0.01}$ | 44 | 55 | 85 | 25 | 24 | 31 |

**3.4. Effect of La Doping on De/Hydrogenation Thermodynamics.** Compared with the hydrogenation capacity of the hydrogenation kinetics, the hydrogenation capacity in the PCT curves, due to the longer hydrogenation time and higher equilibrium pressure, has a higher hydrogen absorption capacity. As shown in the PCT curves (Figure 6), the practical hydrogenation capacity of the Ti−Cr−Mn alloy increases from 1.9 to 2.1 wt % after adding 1 wt % La (Figure 6a). This is because La doping promotes the formation of $LaH_3$ and at the same time reduces the plateau pressure of the
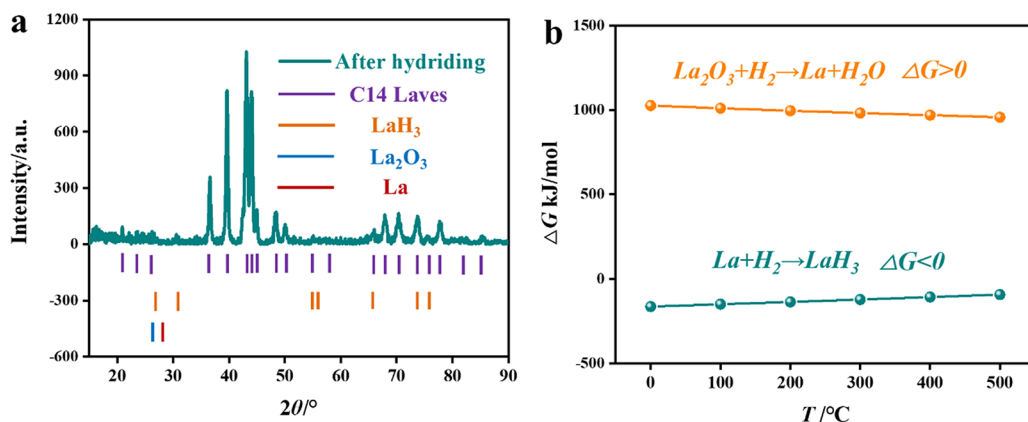


**Figure 5.** (a) XRD pattern of the hydriding $Ti_{1.01}Cr_{0.84}Mn_{0.84}La_{0.01}$ alloy and (b) $\Delta G$ change during the hydriding process of La and $La_2O_3$.
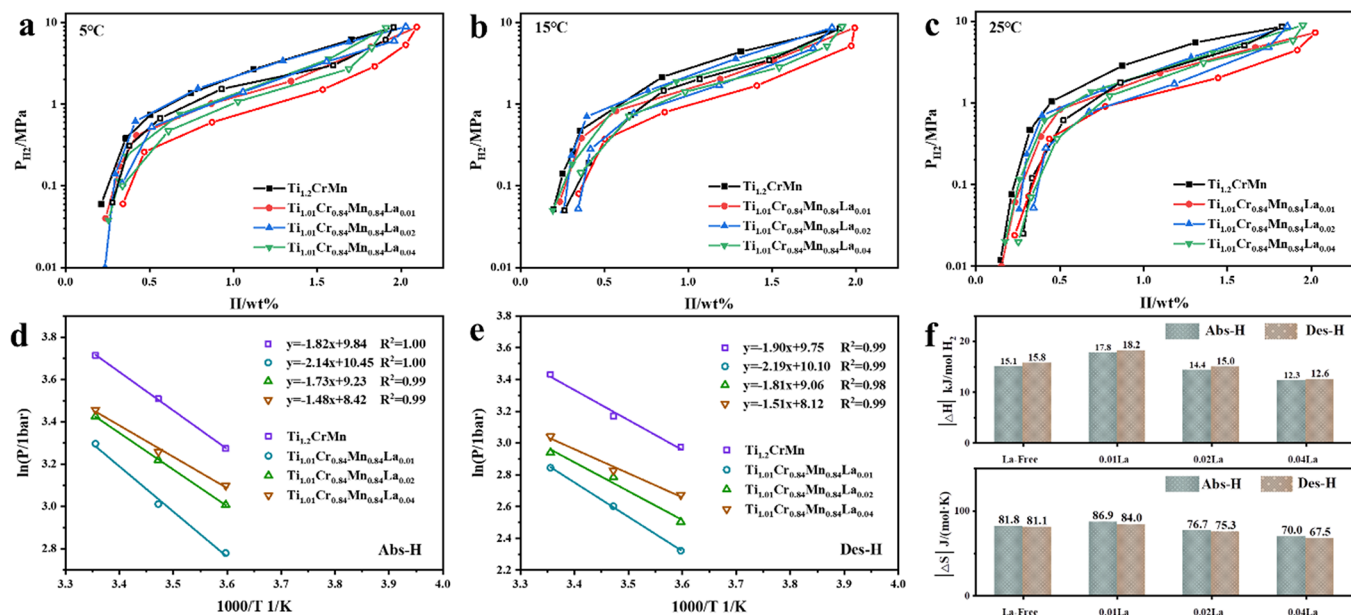
**Figure 6.** Effect of different La doping contents on PCT curves: (a) 5 °C, (b) 15 °C, and (c) 25 °C; van't Hoff plots of alloys: (d) hydrogenation, (e) dehydrogenation, and (f) $\Delta H$ and $\Delta S$ values upon de/hydrogenation.

**Table 3. Effect of La Doping on Plateau Pressure and Slope at 5 °C**

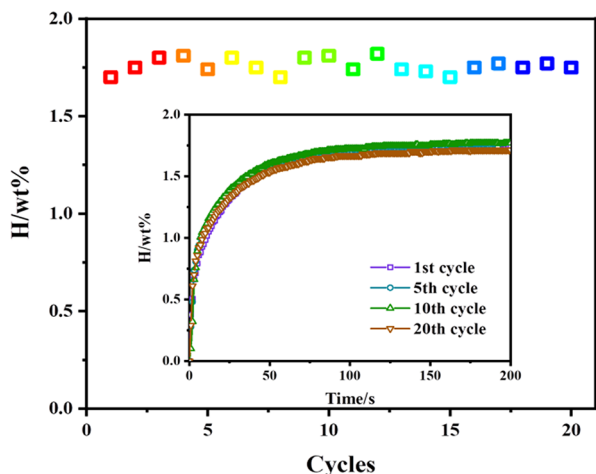| | | $Ti_{1.2}CrMn$ | $Ti_{1.01}Cr_{0.84}Mn_{0.84}La_{0.01}$ | $Ti_{1.01}Cr_{0.84}Mn_{0.84}La_{0.02}$ | $Ti_{1.01}Cr_{0.84}Mn_{0.84}La_{0.04}$ |
|---|---|---|---|---|---|
| Abs-H | $P_{eq}$/MPa | 2.63 | 1.61 | 2.02 | 2.22 |
| | $S_f$ | 1.71 | 2.20 | 2.44 | 3.07 |
| Des-H | $P_{eq}$/MPa | 1.96 | 1.02 | 1.22 | 1.45 |
| | $S_f$ | 1.60 | 2.12 | 2.32 | 2.72 |



**Figure 7.** Cyclic property of the $Ti_{1.01}Cr_{0.84}Mn_{0.84}La_{0.01}$ alloy.

alloy, resulting in the increase in hydrogenation capacity under the limited pressure (<10 MPa). However, the hydrogenation capacity of the sample decreases with sequential increasing of La content. It is ascribed to the fact that the addition of La, resulting in the formation of high-melting-point $La_2O_3$, causes compositional inhomogeneity. The poor homogeneity of the alloy would increase the lattice stress and tilt the hydrogen des/absorption plateau of the alloy. The change of the lattice stress of the main peak of the alloy also resulted in the same conclusion in the previous XRD characterization. The change of the hydrogen des/absorption plateau of the La-doped alloy was calculated in Figure 6d,e and Table 3. It is concluded that

with the increase of La addition, the plateau becomes inclined ($S_f$ becomes larger), hydrogen absorption decreases, and platform pressure increases. Furthermore, it is verified by the van't Hoff equation, and the $\Delta H$ and $\Delta S$ of the alloy upon de/hydrogenation are calculated. Figure 6f demonstrates that the $\Delta H$ change of the alloy is consistent with the corresponding shift in plateau pressure, and the dehydrogenation $\Delta H$ of the $Ti_{1.01}Cr_{0.84}Mn_{0.84}La_{0.01}$ alloy is ~18.2 kJ/mol. The higher the platform pressure is, the easier it is for the alloy to decompose, and the less heat is released by hydrogen absorption or absorption. The $\Delta S$ first increased and then decreased with the increase of La doping content, showing the same change trend as the $\Delta H$.

**3.5. Effect of La Doping on Cyclic Property.** The cyclic property of the $Ti_{1.01}Cr_{0.84}Mn_{0.84}La_{0.01}$ alloy was tested by hydrogenation kinetics at 25 °C. Under the initial hydrogen absorption pressure of 8.0 MPa, the equilibrium pressure is just ~6.0 MPa, lower than the equilibrium pressure in the PCT curve (~8.0 MPa). Thus, the maximum hydrogen absorption capacity in hydrogen absorption kinetics, due to the high plateau pressure of the alloy, is lower than the maximum hydrogen absorption in the PCT curve. By comparing the hydrogen absorption kinetics of the alloy at the 1st, 5th, 10th, and 20th cycles (Figure 7), it is found that the hydrogen absorption rate increases with the increase of cycles, but there is no pronounced effect on the de/hydrogenation performance. Figure 7 demonstrates that the $Ti_{1.01}Cr_{0.84}Mn_{0.84}La_{0.01}$ alloy exhibits excellent cyclic properties. It was concluded that the presence of a La-rich phase could weaken the lattice expansion of the C14 Laves phase and enhance the cycle stability.

# 4. CONCLUSIONS

The effect of Cr/Mn ratio and La doping on the hydrogen performance of Ti−Cr−Mn alloys was studied, and following are the conclusions:

(1) All samples consist of the main C14 Laves phase with a lattice parameter of nearly 0.49/0.80 ($a/c$) nm. The doping of La exhibits a slight influence on the lattice parameter of the C14 Laves phase and precipitates as La and $La_2O_3$.

(2) The La-doped alloy achieves significantly enhanced catalytic activities, kinetics, and stabilities. The hydrogenation kinetics of the La-doped alloy exhibits more rapid hydrogenation kinetics than the La-free alloy. It is ascribed to the fact that La reacts preferentially with hydrogen to form hydride, which provides a fast channel for hydrogen atoms to enter the alloy matrix.

(3) The $\Delta H$ of the La-doped alloy was calculated by the van't Hoff equation and PCT curves to be ∼18.2 kJ/mol. The cycle test proves that the $Ti_{1.01}Cr_{0.84}Mn_{0.84}La_{0.01}$ alloy after La doping exhibits excellent durability due to La addition favoring the chemical homogeneity and reducing the lattice stress.

## ■ AUTHOR INFORMATION

### Corresponding Author

**Qingjun Chen** − *Ganjiang Innovation Academy, Chinese Academy of Sciences, Ganzhou 341000, China;* ● orcid.org/0000-0003-4225-3885; Email: qjchen@gia.cas.cn

### Authors

**Hanbing Zhang** − *State Grid Lishui Power Supply Company, Lishui 323000, China*

**Jichao Ye** − *State Grid Lishui Power Supply Company, Lishui 323000, China*

**Xiaogang Wu** − *State Grid Lishui Power Supply Company, Lishui 323000, China*

**Xinwei Hu** − *State Grid Lishui Power Supply Company, Lishui 323000, China*

**Huazhou Hu** − *Ganjiang Innovation Academy, Chinese Academy of Sciences, Ganzhou 341000, China;* ● orcid.org/0000-0002-7264-9875

**Chuanming Ma** − *Ganjiang Innovation Academy, Chinese Academy of Sciences, Ganzhou 341000, China*

Complete contact information is available at:
https://pubs.acs.org/10.1021/acsomega.2c03367

### Notes

The authors declare no competing financial interest.

## ■ REFERENCES

(1) Hassan, I. A.; Ramadan, H. S.; Saleh, M. A.; Hissel, D. Hydrogen storage technologies for stationary and mobile applications: Review, analysis and perspectives. *Renewable Sustainable Energy Rev.* **2021**, *149*, No. 111311.

(2) Ding, N.; Li, Y.; Liang, F.; Liu, B.; Liu, W.; Wang, Q.; Wang, L. Highly efficient hydrogen storage capacity of 2. 5 wt % above 0.1 MPa using Y and Cr codoped V-based alloys. *ACS Appl. Energy Mater.* **2022**, *5*, 3282−3289.

(3) Cao, Z.; Ouyang, L.; Wang, H.; Liu, J.; Sun, L.; Felderhoff, M.; Zhu, M. Development of Zr-Fe-V alloys for hybrid hydrogen storage system. *Int. J. Hydrogen Energy* **2016**, *41*, 11242−11253.

(4) Hu, H.; Ma, C.; Chen, Q. Mechanism and microstructural evolution of TiCrVFe hydrogen storage alloys upon de−/hydrogenation. *J. Alloys Compd.* **2021**, *877*, No. 160315.

(5) Salman, M. S.; Rambhujun, N.; Pratthana, C.; Srivastava, K.; Aguey-Zinsou, K. F. Catalysis in Liquid Organic Hydrogen Storage: Recent Advances, Challenges, and Perspectives. *Ind. Eng. Chem. Res.* **2022**, *61*, 6067−6105.

(6) Ouyang, L.; Huang, J.; Wang, H.; Liu, J.; Zhu, M. Progress of hydrogen storage alloys for Ni-MH rechargeable power batteries in electric vehicles: A review. *Mater. Chem. Phys.* **2017**, *200*, 164−178.

(7) Wang, C. C.; Zhou, Y. T.; Yang, C. C.; Jiang, Q. Clarifying the capacity deterioration mechanism sheds light on the design of ultra-long-life hydrogen storage alloys. *Chem. Eng. J.* **2018**, *352*, 325−332.

(8) Ulmer, U.; Dieterich, M.; Pohl, A.; Dittmeyer, R.; Linder, M.; Fichtner, M. Study of the structural, thermodynamic and cyclic effects of vanadium and titanium substitution in laves-phase AB2 hydrogen storage alloys. *Int. J. Hydrogen Energy* **2017**, *42*, 20103−20110.

(9) Chen, Y.; Chen, R. R.; Yu, K.; Ding, X.; Li, X. Z.; Ding, H. S.; Su, Y. Q.; Guo, J. J. Effect of Ce substitution on hydrogen absorption/desorption of Laves phase-related BCC solid solution $Ti_{33}V_{37}Mn_{30}$ alloy. *J. Alloys Compd.* **2019**, *783*, 617−624.

(10) Dixit, V.; Huot, J. Investigation of the microstructure, crystal structure and hydrogenation kinetics of Ti-V-Cr alloy with Zr addition. *J. Alloys Compd.* **2019**, *785*, 1115−1120.

(11) Tousignant, M.; Huot, J. Hydrogen sorption enhancement in cold rolled $LaNi_5$. *J. Alloys Compd.* **2014**, *595*, 22−27.

(12) Nakamura, R.; Asano, K.; Yoshimi, K.; Iijima, Y. Thermal analysis of lattice defects in $LaNi_5$. *J. Alloys Compd.* **2006**, *413*, 211−213.

(13) Hu, H.; Ma, C.; Chen, Q. Improved hydrogen storage properties of $Ti_2CrV$ alloy by Mo substitutional doping. *Int. J. Hydrogen Energy* **2022**, *47*, 11929−11937.

(14) Yu, X. B.; Chen, J. Z.; Wu, Z.; Xia, B. J.; Xu, N. X. Effect of Cr content on hydrogen storage properties for Ti-V-based BCC-phase alloys. *Int. J. Hydrogen Energy* **2004**, *29*, 1377−1381.

(15) Zhu, W.; Ren, L.; Lu, C.; Xu, H.; Sun, F.; Ma, Z.; Zo, J. Nanoconfined and in situ catalyzed $MgH_2$ self-assembled on 3D $Ti_3C_2$ MXene folded nanosheets with enhanced hydrogen sorption performances. *ACS Nano* **2021**, *15*, 18494−18504.

(16) Liang, L.; Wang, C.; Ren, M.; Li, S.; Wu, Z.; Wang, L.; Liang, F. Unraveling the synergistic catalytic effects of $TiO_2$ and $Pr_6O_{11}$ on superior dehydrogenation performances of $\alpha$-$AlH_3$. *ACS Appl. Mater. Interface* **2021**, *13*, 26998−27005.

(17) Matsunaga, T.; Buchter, F.; Mauron, P.; Bielman, M.; Nakamori, Y.; Orimo, S.; Ohba, N.; Miwa, K.; Towata, S.; Züttel, A. Hydrogen storage properties of $Mg[BH_4]_2$. *J. Alloys Compd.* **2008**, *459*, 583−588.

(18) Hu, Y. H.; Ruckenstein, E. Ultrafast reaction between $Li_3N$ and $LiNH_2$ to prepare the effective hydrogen storage material $Li_2NH$. *Ind. Eng. Chem. Res.* **2006**, *45*, 4993−4998.

(19) Kaye, S. S.; Dailly, A.; Yaghi, O. M.; Long, J. R. Impact of preparation and handling on the hydrogen storage properties of $Zn_4O$ (1,4-benzenedicarboxylate)$_3$ (MOF-5). *J. Am. Chem. Soc.* **2007**, *129*, 14176−14177.

(20) Li, Z.; Yu, J. Z.; Zhang, Y.; Liu, D. M.; Wang, C. Y.; Si, T. Z.; Li, Y. T.; Zhang, Q. A. Coupling of nanoconfinement with metallic catalysis in supported $NaAlH_4$ for low-temperature hydrogen storage. *J. Power Sources* **2021**, *491*, No. 229611.

(21) Huang, T.; Huang, X.; Hu, C.; Wang, J.; Liu, H. B.; Xu, H.; Sun, F. Z.; Ma, Z. W.; Zou, J. X.; Ding, W. J. MOF-derived Ni nanoparticles dispersed on monolayer MXene as catalyst for improved

hydrogen storage kinetics of MgH$_2$. *Chem. Eng. J.* **2021**, *421*, 1385−8947.

(22) Chen, K.; Ouyang, L.; Zhong, H.; Liu, J.; Wang, H.; Shao, H.; Zhang, Y.; Zhu, M. Converting H$^+$ from coordinated water into H$^−$ enables super facile synthesis of LiBH$_4$. *Green Chem.* **2019**, *21*, 4380−4387.

(23) Zhu, Y.; Ouyang, L.; Zhong, H.; Liu, J.; Wang, H.; Shao, H.; Huang, Z.; Zhu, M. Closing the loop for hydrogen storage: Facile regeneration of NaBH$_4$ from its hydrolytic product. *Angew. Chem., Int. Ed.* **2020**, *59*, 8623−8629.

(24) Ouyang, L.; Chen, W.; Liu, J.; Felderhoff, M.; Wang, H.; Zhu, M. Enhancing the Regeneration Process of Consumed NaBH$_4$ for Hydrogen Storage. *Adv. Energy Mater.* **2017**, *7*, No. 1700299.

(25) Cao, Z.; Ouyang, L.; Wang, H.; Liu, J.; Sun, D.; Zhang, Q.; Zhu, M. Advanced high-pressure metal hydride fabricated via Ti-Cr-Mn alloys for hybrid tank. *Int. J. Hydrogen Energy* **2015**, *40*, 2717−2728.

(26) Cao, Z.; Ouyang, L.; Wang, H.; Liu, J.; Sun, L.; Zhu, M. Composition design of Ti−Cr−Mn−Fe alloys for hybrid high-pressure metal hydride tanks. *J. Alloys Compd.* **2015**, *639*, 452−457.

(27) Suwarno, S.; Dicky, G.; Suyuthi, A.; Effendi, M.; Witantyo, W.; Noerochim, L.; Ismail, M. Machine learning analysis of alloying element effects on hydrogen storage properties of AB$_2$ metal hydrides. *Int. J. Hydrogen Energy* **2022**, *47*, 11938−11947.

(28) Osumi, Y.; Suzuki, H.; Kato, A.; Oguro, K.; Sugioka, T.; Fujita, T. Hydrogen storage properties of Ti$_{1+x}$C$_{r2-y}$Mn$_y$ alloys. *J. Less Common Met.* **1983**, *89*, 257−262.

(29) Agresti, F.; Lo Russo, S.; Maddalena, A.; Principi, G.; Mazzolai, G.; Coluzzi, B.; Biscarini, A.; Mazzolai, F. M.; Tuissi, A. Reaction of hydrogen with the Laves phase (C14) TiCr$_{1.78−x}$Mn$_x$ compounds. *Mater. Sci. Eng., A* **2009**, *521−522*, 143−146.

(30) Nong, Z. S.; Zhu, J. C.; Yang, X. W.; Cao, Y.; Lai, Z. H.; Liu, Y.; Sun, W. First-principles calculations of the stability and hydrogen storage behavior of C14 Laves phase compound TiCrMn. *Solid State Sci.* **2014**, *32*, 1−7.

(31) Liu, X. P.; Cuevas, F.; Jiang, L. J.; Latroche, M.; Li, Z. N.; Wang, S. M. Improvement of the hydrogen storage properties of Ti−Cr−V−Fe BCC alloy by Ce addition. *J. Alloys Compd.* **2009**, *476*, 403−407.

(32) Li, W.; Wu, E.; Ma, P.; Sun, K.; Chen, D. Hydrogen storage properties of Ti$_{1-x}$Sc$_x$MnCr Laves phase alloys. *Int. J. Energy Res.* **2013**, *37*, 686−697.

(33) Zhou, L.; Li, W.; Hu, H.; Zeng, H.; Chen, Q. Ce-doped TiZrCrMn alloys for enhanced hydrogen storage. *Energy Fuels* **2022**, *36*, 3997−4005.

(34) Rietveld, H. M. A profile refinement method for nuclear and magnetic structures. *J. Appl. Crystallogr.* **1969**, *2*, 65.